THE JOURNAL OF PHYSICAL CHEMISTRY B

 VOLUME 106, NUMBER 21, MAY 30, 2002

FEATURE ARTICLE

Aqueous Solution/Air Interfaces Probed with Sum Frequency Generation Spectroscopy

Mary Jane Shultz*, Steve Baldelli,† Cheryl Schnitzer,‡ and Danielle Simonelli§

Department of Chemistry, Pearson Lab., Tufts University, Medford, Massachusetts 02155

Received: December 10, 2001; In Final Form: February 21, 2002

An important issue for developing a molecular-level mechanism of heterogeneous interactions at the aqueous interface is determining changes in the interface with changes in the bulk composition. Development of the nonlinear spectroscopy, sum frequency generation (SFG) provides a technique to probe these changes. Several molecular and ionic solutes have been used to investigate changes in the structure of the aqueous interface. Molecular solutes include glycerol and ammonia. Ionic and associated ion complexes include sulfuric acid as well as alkali sulfate and bisulfate salts. Molecular solutes and associated ion complexes penetrate to the top monolayer of the aqueous-air interface displacing water from the interface. Specifically, the conjectured ammonia−water complex is observed with ammonia tilted, on average, 25−38° from the normal. Ionic solutes generate a double layer in the interfacial region due to the differential distribution of anions and cations near the interface. The strength of the double layer is dependent on ion size and charge. Due to the extreme size of the proton, the strongest field is generated by acidic solutes. As the ionic solute concentration increases, associated ion pairs form and these penetrate to the top monolayer. These results have wide implications because the aqueous interface is ubiquitous in atmospheric and biological systems.

1. Introduction

Aqueous solution interfaces are ubiquitous, playing important roles in phenomena as diverse as transport across cell membranes, corrosion, the origin of life, and adsorption and reaction of gas-phase molecules in the atmosphere. One of the keys to unraveling phenomena involving aqueous interfaces is understanding how interfacial water adapts to the presence of substances in solution and at the interface. Conversely, the structure of molecules at the aqueous solution interface affects interactions between these molecular substances and incoming potential reactants.

A molecular-level understanding of the aqueous surface and its response to solutes is a long-standing objective, yet there is no comprehensive model that describes the wide range of macroscopic and microscopic properties of aqueous solutions.[1] Molecular-level, experimental data about the surface is scarce due to a combination of a low number density and the high vapor pressure, dynamic nature of the interface. Theoretical simulations are severely challenged by the cooperativity and flexibility of the hydrogen bonding network. Small cluster studies, both theoretical[2,3] and experimental[4−8] serve as prototypes for solutions and have provided valuable insights. The results suggest that cations are symmetrically hydrated in the interior of a cluster, whereas anions tend to be on the surface for small clusters. The location of anions such as Cl^- are particularly relevant to understanding the oxidative load of the troposphere in coastal areas. The accessibility of the chloride ion greatly affects the mechanism of interaction of gas-phase species such as HNO_3 with sea salt aerosols[9−13] and the subsequent chlorine evolution rate. Similarly, the surface

† Department of Chemistry, University of Houston, Houston, TX 77204.
‡ Department of Chemistry, Stonehill College, North Easton, MA 02357.
§ Intel Corporation, Ronler Acres, 2501 NW 229th Street, Hillsboro, OR 97124-6497.

10.1021/jp014466v CCC: $22.00
Published on Web 05/04/2002

composition of polar stratospheric clouds affects the rate of relevant heterogeneous reactions. For example, the reactions[14−17]

$$N_2O_{5(g)} + H_2O_{(a)} \rightarrow 2\ HNO_{3(a,g)} \quad (1)$$

$$ClONO_{2(g)} + H_2O_{(a)} \rightarrow HOCl_{(g)} + HNO_{3(a,g)} \quad (2)$$

$$ClONO_{2(g)} + HCl_{(a)} \rightarrow Cl_{2(g)} + HNO_{3(a,g)} \quad (3)$$

are believed to play a role in heterogeneous ozone destruction. Although these reactions along with others account for the major features of the observed variation in polar ozone concentrations, smaller features indicate gaps in the model. The key question is, are these processes heterogeneous surface reactions or are they homogeneous, bulk-phase reactions? Surface reactions will be directly affected by the molecular orientation and distribution at the interface, whereas bulk reactions will depend indirectly on the surface features because impinging gas-phase species need to penetrate this surface.

Due to the importance of the aqueous interface, water surfaces have been studied since the earliest days of physical chemistry.[18−24] Methods such as surface potential and surface tension,[25] although not molecular-level measurements, have contributed valuable insights into surfaces. More recently, methodologies from the study of solid surfaces (e.g., ion scattering,[26] molecular and atom scattering,[27−30] and Auger and X-ray photoelectron spectroscopy[31−33]) have been extended to study liquid interfaces. With the advent of nonlinear spectroscopic methods, discussed below, the tools are now available to probe a much larger variety of soft interfaces with molecular specificity at the monolayer level. It is now possible to describe the structure of water at the neat interface, to probe the molecular distribution on the surface of ternary and more complex interfaces, and to investigate perturbation of the structure of water by dissolved inorganic ions in solution.

2. Surface Specific Detection at Liquid Interfaces

Despite the importance of high-vapor pressure surfaces, including the aqueous solution interface, a molecular-level picture of the configuration and distribution of substances at these interfaces was lacking until recently. The challenge lies in probing the surface without perturbing it, so spectroscopic techniques are the methods of choice. Yet the wavelength of most spectroscopic methods is sufficiently long that obtaining the signal due to surface species in the presence of larger numbers in the adjacent bulk phases requires that the surface signal be identified and deconvoluted from that of the bulk phases. Some success has been obtained using single reflectance Fourier transform infrared spectroscopy compared with transmission spectra[34] or comparisons among FTIR spectra of different cluster sizes.[35−39] This article focuses on more generally applicable, surface-specific spectroscopic techniques, providing a picture of surface partitioning of a variety of solutes.

Surface specific spectroscopies developed to date are nonlinear techniques that exploit the inherent breaking of isotropic symmetry at the interface and consist of second harmonic generation (SHG) and sum frequency generation (SFG). SHG doubles the frequency of the input light, usually in the visible region of the spectrum, and is species specific if the electronic resonances are well separated. Because electronic resonances are generally broad, the related technique, SFG, is the more versatile choice for probing surfaces comprised of a mixture. To attain this generality, SFG typically sums an infrared and a visible frequency (Figure 1). Scanning the infrared yields the vibrational signature of the surface molecules. General implementation of SFG awaited development of reliable, pulsed infrared laser beams that have only become available in the past decade-and-a-half.

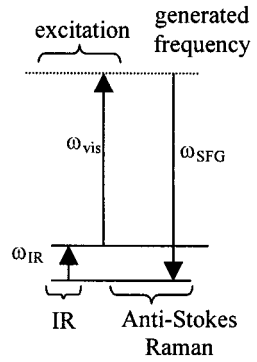

Figure 1. Energy-level diagram schematic of the sum frequency generation process.

3. Sum Frequency Generation

Probing a liquid interface is challenging due to the inherently dynamic nature of the surface. For example, at 0 °C, the vapor pressure of water (∼4.5 Torr) results in exchange between the gas phase and the surface of about three million monolayers per second. It is thus surprising that a spectrum of the surface contains features other than broad bands due to the ever-changing environment. The resonances therefore reflect the orientational effect of the asymmetric environment at the interface.

In the 1960s, Bloembergen and Pershan[40] set out the basis for the two nonlinear techniques and several reviews have since appeared in the literature.[41−45] The first successful application of nonlinear spectroscopy to liquid interfaces involved *p*-nitrobenzoic acid, reported by Shen et al. in the 1980s.[46] Because *p*-nitrobenzoic acid is a molecule with a strongly directed, visible resonance, analysis of the SHG polarization characteristics yields orientation and number density at the interface. Accessing a molecular resonance is the basis for tuning the input frequency such that the fundamental or second harmonic is in resonance with an electronic state.[47] The first reported SHG of a neat liquid interface is that of water reported by Eisenthal et al.[48] Analysis of the polarization dependence of SHG from interfacial water indicates that the average dipole moment vector is nearly parallel to the interface and on average, the hydrogen atoms are oriented slightly below the surface.

Either accessing a visible resonance or probing only neat interfaces limits the technique. However, applicability is generalized if two input frequencies are used—one in the infrared and one in the visible region—because the vibrational signature is characteristic of specific bonded groups and vibrational resonances shift in response to perturbation of this bonding. The general applicability of SFG comes at the cost of experimental complexity. To assess the feasibility of the technique, the first SFG experiments, reported in 1987-88, optimized the surface concentration and limited bulk penetration by examining organic molecules on solid substrates: quartz[49,50] and semiconductors.[51] Several years later, Shen et al.[52] used SFG to study the neat methanol liquid interface and in 1993 pure water interface.[53] Currently, SFG is the only technique capable of producing vibrational spectra of neat liquid interfaces, liquid−air solution interfaces or buried liquid−liquid interfaces.[54−57]

The nonlinear response of the medium to the incident electromagnetic waves is determined by the hyperpolarizability of the medium.[58−63] To second order, an incident electric field

TABLE 1: Fresnel Factors. *X*, *Y*, and *Z* Refer to the Laboratory Coordinate System, *XZ* is the Plane of Incidence and *XY* is the Surface Plane

	L_I(SF)	K(vis)	K (IR)
X	$-\cos\theta_{t,SF}/[\cos\theta_{t,SF}+n_{SF}\cos\theta_{i,SF}]$	$2\cos\theta_{i,\omega1}\cos\theta_{t,\omega1}/[\cos\theta_{t,\omega1}+n_1\cos\theta_{i,\omega1}]$	$2\cos\theta_{i,\omega2}\cos\theta_{t,\omega2}/[\cos\theta_{t,\omega2}+n_2\cos\theta_{i,\omega2}]$
Y	$1/[\cos\theta_{i,SF}+n_{SF}\cos\theta_{t,SF}]$	$2\cos\theta_{i,\omega1}/[\cos\theta_{i,\omega1}+n_1\cos\theta_{t,\omega1}]$	$2\cos\theta_{i,\omega2}/[\cos\theta_{i,\omega2}+n_2\cos\theta_{t,\omega2}]$
Z	$-\sin\theta_{t,SF}/[\cos\theta_{t,SF}+n_{SF}\cos\theta_{i,SF}]$	$-2\cos\theta_{i,\omega1}\sin\theta_{t,\omega1}/[\cos\theta_{t,\omega1}+n_1\cos\theta_{i,\omega1}]$	$-2\cos\theta_{i,\omega2}\sin\theta_{t,\omega2}/[\cos\theta_{t,\omega2}+n_2\cos\theta_{i,\omega2}]$

θ_i = incident angle, θ_t =transmitted angle.

induces a polarization, $\boldsymbol{P}$, in the medium as

$$\boldsymbol{P} = \alpha^{(1)}.\,\boldsymbol{E_1} + \chi^{(2)}\!:\boldsymbol{E_1}\boldsymbol{E_2} \tag{4}$$

where $\alpha^{(1)}$ and $\chi^{(2)}$ are the first and second-order polarizabilities, respectively. The first-order response, $\alpha^{(1)}$, is a matrix that describes Rayleigh and Raman scattering. The second-order response is a tensor which is the focus of this discussion. The observed intensity is proportional to the absolute square of the polarization, and the square is the source of interferences that can complicate spectra. Equation 4 implies that there are two relationships that must be considered in order to understand this second-order response. One is the relationship of the electric fields, $\boldsymbol{E}_1$ and $\boldsymbol{E}_2$ in the nonlinear medium to the incident fields. The other is the relationship of the second-order polarizability tensor, $\chi^{(2)}$, to the molecules in the surface. Each of these relationships is described below.

3.1. Optical Factors and Electric Fields. The electric fields in the medium are related to the incident fields by Fresnel factors that reflect the efficiency for coupling into the nonlinear medium. There is a similar optical factor for coupling out the generated sum frequency. These factors result from the boundary condition that the tangential component of the electric field is continuous across a boundary. The visible ($\boldsymbol{E}_J$) and infrared ($\boldsymbol{E}_K$) fields in the medium are related to the input fields by

$$\boldsymbol{E}_J(\text{vis}) = K_J(\text{vis})e^{\circ}_{\text{vis}};\ \boldsymbol{E}_K(\text{IR}) = K_J(\text{IR})e^{\circ}_{\text{IR}} \tag{5}$$

The Fresnel factors: K_J(vis), K_K(IR) are listed in Table 1 and e°_{vis} (e°_{IR}) is the incident visible (infrared) field. A similar nonlinear optical factor, L_I(SF) (Table 1), defines the generated sum frequency field, $\boldsymbol{E}_I(\text{SF}) = L_I(\text{SF})$.

The sum frequency angle, θ_{SF}, is determined by momentum matching at the interface

$$n_{SF}^2\omega_{SF}^2\sin^2\theta_{SF} = n_1^2\omega_1^2\sin^2\theta_1 + n_2^2\omega_2^2\sin^2\theta_2 + 2n_1n_2\omega_1\omega_2\sin\theta_1\sin\theta_2 \tag{6}$$

The Fresnel factors reduce the electric fields and, for the *ppp* polarization combination, interference between components results in alteration or cancellation of expected intensity.

3.2. Nonlinear Susceptibility. The relationship between the surface nonlinear susceptibility, χ_{IJK}, and the molecular hyperpolarizability, β_{abc}, depends on the molecular orientation. The link between molecular orientation and surface susceptibility is commonly analyzed using Euler angle relationships among four coordinate systems: the laboratory system (*XYZ*) that defines the plane of incidence, the surface system (*xyz*) that defines the surface normal, the molecular Cartesian system (*abc*), and the molecular normal coordinates (*ABC*). The general results of these transformations are given in the literature.[60,61] The Cartesian susceptibility elements are related to the normal coordinate elements as

$$\beta_{abc} = \frac{1}{n}\sum_{\text{orientations}}\beta_{abc} \tag{7}$$

where n is the number of equivalent orientations. The Cartesian coordinate susceptibilities are similarly projected onto the surface coordinate system and averaged over the equivalent

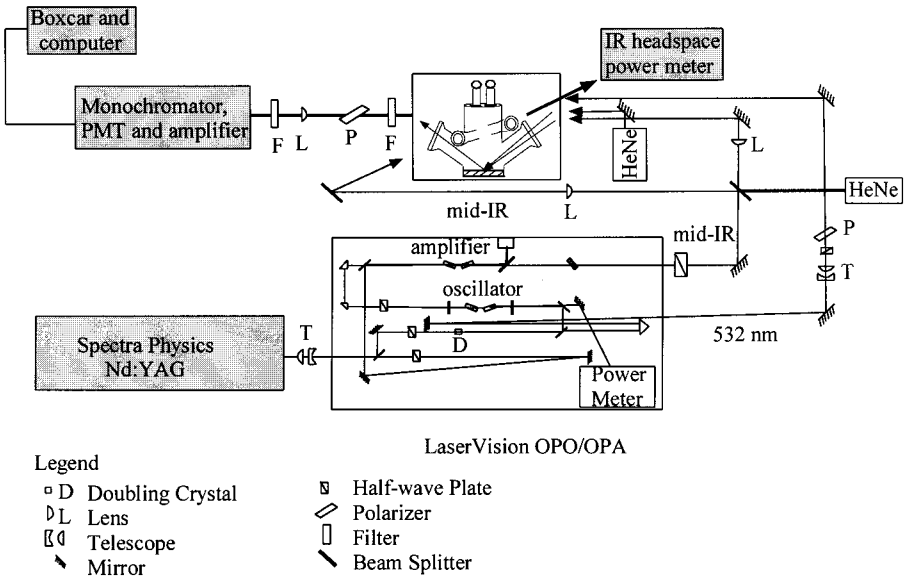

Figure 2. Schematic of experimental apparatus for sum frequency generation. Nonlinear processes in the optical parametric oscillator/optical parametric amplifier generate the infrared beam. In the oscillator stage, nonlinear processes in the KTA crystals parametrically split the 532 nm pump into a signal and an idler beam. Mid-IR is generated in the amplifier stage by difference frequency mixing the idler with a 1064-nm beam. The 532-nm visible beam is generated by doubling the YAG fundamental in a KTP crystal. The infrared and visible beams are brought to a gentle focus beyond the liquid surface. The generated sum frequency is filtered and focused on the entrance slit of a monochromator, detected by a photomultiplier tube and sent to a boxcar and computer for analysis. The master clock is the 1064-nm pulse from the Nd:YAG laser.

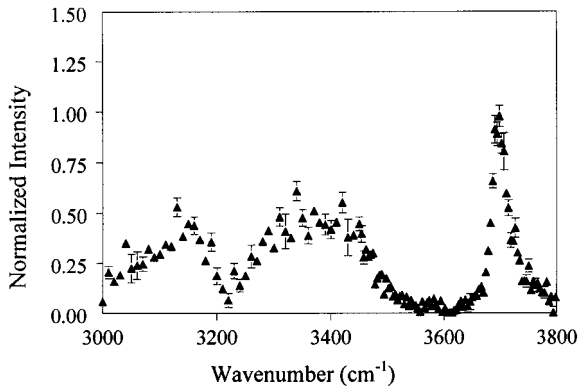

Figure 3. Sum frequency generation spectrum of neat air/water interface at 0 °C obtained with *ssp* polarization.

surface orientations

$$\chi_{IJK} = N\langle\beta_{IJK}\rangle \tag{8}$$

where N is the number of molecules and $\langle ... \rangle$ denotes the orientational average. For a two-dimensional, isotropic surface the orientational average results in zero intensity for *sss*, *spp*, *psp*, and *pps* polarizations. Finally, the SFG signal intensity is proportional to the polarization squared

$$\text{signal intensity} \propto |P|^2 \propto |\chi^{(2)}|^2 = N^2|\langle\beta^{(2)}\rangle|^2 \tag{9}$$

resulting in an SFG intensity that is proportional to the square of the number of molecules contributing to the signal modulated by the average orientation. Specifically for the work discussed below, with the *ssp* polarization combination, the SFG intensity is strongly affected by the projection of the infrared dipole onto the surface normal.

3.3. Experimental Section. A schematic of the experiment is shown in Figure 2. The objective is to overlap pulsed visible and infrared beams in space and time on the liquid interface. Here, the source of the pulsed visible beam is a 1064-nm pulse from a *n*sec. Nd:YAG laser (Spectra-Physics GCR150) doubled in a KTP crystal. The infrared beam is generated in the optical parametric oscillator, optical parametric amplifier (OPO/OPA) by parametrically splitting the 532-nm beam into a signal and an idler beam in the OPO stage and difference frequency mixing the idler with 1064 nm in the OPA stage. The polarization of both the visible and infrared beams is rotated as required. The two beams are collinearly focused to a spot beyond the liquid interface. Energy density is 100 mJ cm^{-2} for the infrared and 400 mJ cm^{-2} for the visible light. A portion of the infrared beam is split off prior to the sample and sent through the headspace to monitor the infrared intensity reaching the surface. All spectra discussed here are normalized to the infrared intensity and referenced to the free-OH stretch of water, assigned unit intensity.

4. Neat Water

The point of departure for discussing aqueous solution interfaces is the spectrum of the neat air−water interface. The spectrum in Figure 3 is consistent with the first SFG spectrum of water published by Shen et al.[53] Three major features are apparent: a sharp peak at 3700 cm^{-1} and two broader peaks centered at approximately 3400 and 3150 cm^{-1}. Although details of the water spectra vary somewhat with acquisition parameters, e.g., visible excitation wavelength and incident angles, all share these three features. Interpretation of the 3700 cm^{-1} peak is the most straightforward and noncontroversial. Midway between the symmetric and antisymmetric gas-phase absorptions of water, 3700 cm^{-1} corresponds to the decoupled OH oscillator frequency. It is thus assigned to an OH stretch of surface water molecules with a hydrogen free of hydrogen bonding, dubbed the "free-OH" or "dangling-OH" stretch. To be free of hydrogen bonding, the hydrogen atom must protrude from the surface. Significantly for the work discussed here, these OH bonds are necessarily in the topmost monolayer of the surface, and perturbation of this peak reflects changes in the top monolayer.

Interpretation of the remaining two, hydrogen-bonded peaks remains controversial.[64,65] The lower frequency peak is variously termed the structured peak, the ice-like peak, or the symmetric stretch of symmetrically bonded water. These characterizations stem from the similar characterization of Raman spectra of water, ice, and aqueous solutions.[66−72] Conversely, the peak at 3400 cm^{-1} is attributed to disordered water at the surface in analogy to the prominent feature in the Raman spectrum of structure breaking ions. An alternate characterization is based on theoretical calculations for ice[37,39,73−75] and water clusters.[76] The lower frequency peak is attributed to those water molecules that are strongly hydrogen bonded and include those for which the other OH bond is dangling. In this interpretation, the 3400 cm^{-1} peak is due to more weakly hydrogen-bonded OH bonds. These alternate interpretations present somewhat different pictures of water. Resolution of the controversy over the interpretation awaits further experimental and theoretical investigation. In this discussion, the lower frequency peak is referred to as the stronger hydrogen-bonded peak and the 3400 cm^{-1} peak as the weaker hydrogen-bonded peak.

5. Aqueous Solutions

5.1. First Layer: Free OH. Three molecules that have been used to probe the response of the first monolayer of water to added solutes are discussed here: glycerol,[77] sulfuric acid,[78−81] and ammonia.[82,83] Glycerol is chosen because it forms an ideal solution with water, sulfuric acid is selected due to its atmospheric relevance, and ammonia is an excellent test-probe molecule for the aqueous surface. Related investigations with sulfate and bisulfate salts are presented with the sulfuric acid results.

5.1.1. Aqueous Glycerol. Glycerol is hygroscopic: yet glycerol and water form a nearly ideal solution.[84] SFG is an excellent probe technique for the molecular distribution on the aqueous glycerol surface because both molecules are independently detected: glycerol in the CH stretch region and water in the free-OH region. Ideality suggests that glycerol and water do not greatly perturb each other. The spectra are shown in Figure 4 with mole fraction, x, of glycerol decreasing down each column. The glycerol resonances at 2882 cm^{-1} (CH_2 symmetric stretch) and 2948 cm^{-1} (CH_2 antisymmetric stretch) remain strong, diminishing only slightly down to 25 mol % glycerol. The glycerol mole fraction must be reduced to 0.10 (Figure 4B) for the intensity to become 50% of that of neat glycerol (surface coverage, 70% if orientation does not change). The free-OH resonance, clearly visible at 0.10x glycerol (Figure 4F) rises (Figure 4G and H) as the glycerol signal decreases (Figure 4C and D).

The neat glycerol signal serves as a calibration of the signal from a full glycerol monolayer. To use this signal for coverage determination at lower concentrations, it is necessary to monitor the glycerol orientation. The symmetric and antisymmetric stretch infrared dipoles are orthogonal, so the orientation determines the intensity ratio for these two peaks. The intensity ratio is constant between 0.1x to 1.0x, thus the orientation does

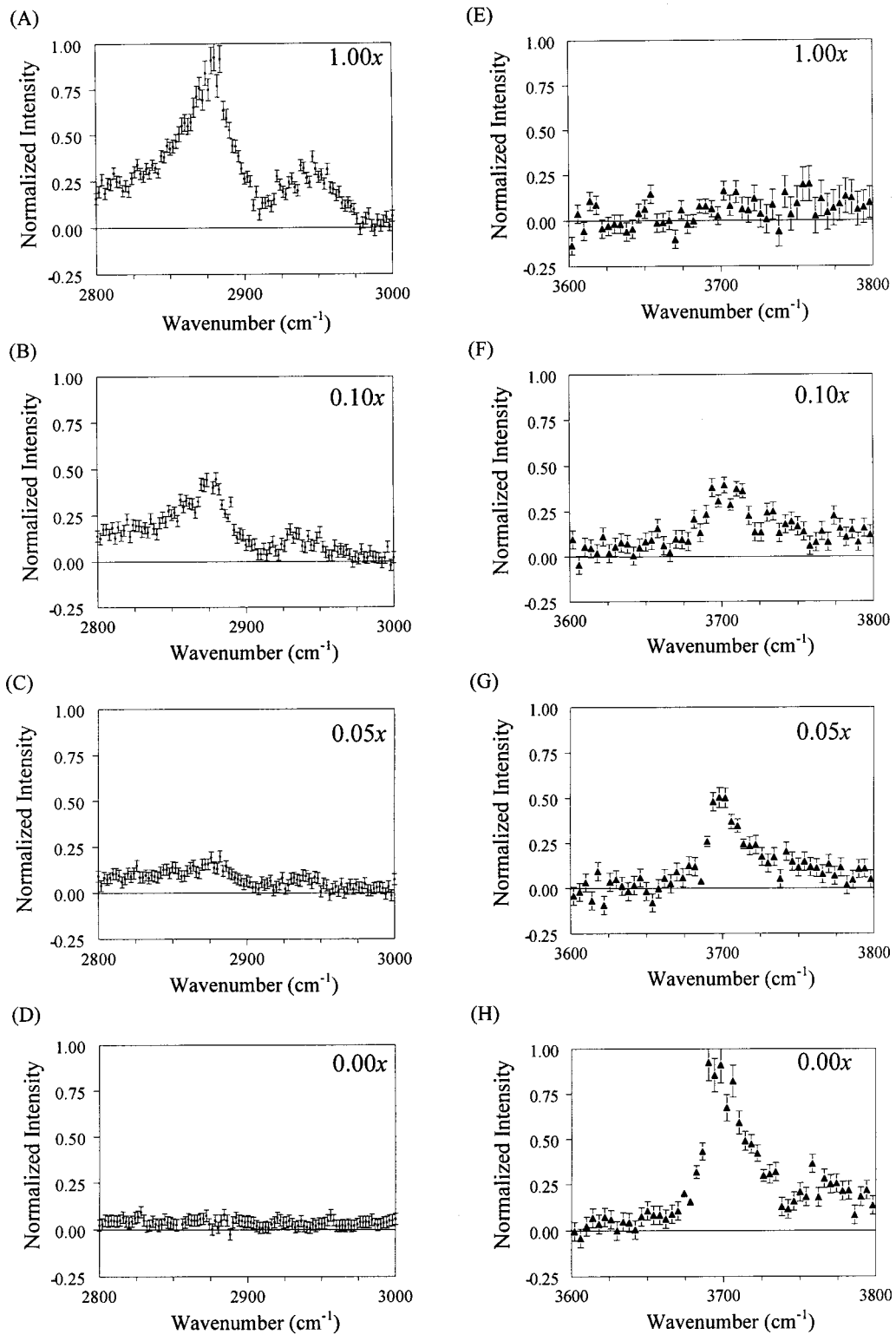

Figure 4. SFG spectra of binary glycerol−water solutions with glycerol mole fraction (x) decreasing down the column: (A), (E) 1.00x; (B), (F) 0.10x; (C), (G) 0.05x; and (D), (H) 0.00x. All solutions at 0 °C, spectra obtained with *ssp* polarization. Spectra A−D indicate glycerol by the C−H stretches, 2800−3000 cm^{-1}. Spectra E−H show the free-OH resonance of water, centered at 3700 cm^{-1}.

not change in this range and the intensity along with the area per glycerol molecule[85] can be used to determine the fraction of the surface covered by glycerol. Similarly, the previously reported calibration of the free-OH signal[53] and the area per water molecule determines the surface covered by water. The entire surface is accounted for at each concentration (Figure 5)[77] and, in agreement with surface tension measurements, the surface mole fraction exceeds that of the bulk, Figure 6. The SFG measurement, however, indicates an even larger excess of glycerol at the surface than is found using surface tension measurements. This result is due to SFG and surface tension measuring different depths of the surface region. SFG detects only the anisotropically ordered layer of the surface, whereas surface tension is a macroscopic measurement. For example, assuming that layers beyond the first monolayer are randomly oriented, SFG indicates that the surface of a 0.5x bulk glycerol

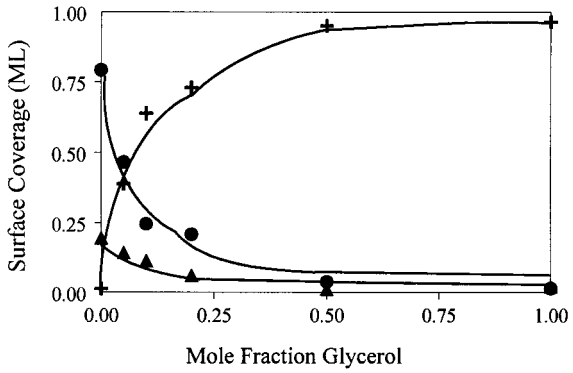

Figure 5. Surface coverage vs bulk mole fraction glycerol: (+) glycerol, (●) hydrogen-bonded water, (▲) free OH.

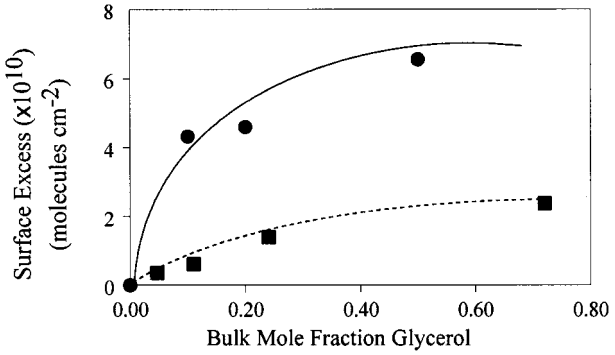

Figure 6. Surface excess glycerol vs bulk mole fraction glycerol: (●) SFG data, (■) surface tension data.

solution contains a 9:1 glycerol-water ratio. The reduced surface tension of a glycerol−water solution results from this first monolayer excess, plus the lower excess in subsequent layers in the gradient toward the bulk mole fraction.

The glycerol concentration in the gas phase is essentially zero at 0 °C because the vapor pressure of glycerol is very small. With the surface concentration of glycerol exceeding that in the bulk, the picture of this hygroscopic surface is as follows. Partitioning of glycerol to the interface indicates that water is energetically favored to be in the interior. A water molecule landing on the surface therefore has a short residence time, either bouncing off the surface or partitioning to the interior of the liquid. This conclusion of water interaction at the interface resulting from measurement of equilibrium surface partitioning is the same as drawn from molecular beam scattering experiments[86] The surface of this ideal mixture is enriched in glycerol and can be viewed as a semipermeable membrane allowing water to pass.

5.1.2. Aqueous Sulfates. Sulfuric acid is among the top chemicals produced annually in the United States; consequently, the aqueous solution surface properties are of wide interest. In addition, sulfuric acid and sulfate aerosols play a central role in atmospheric chemistry as cloud condensation nuclei at all altitudes. Stratospheric sulfate aerosols are the dominant staging surfaces for reactions involved in ozone depletion. One of the primary unknowns for assessing plausible mechanisms for stratospheric processes is determining the distribution and orientation of water on the surface for 40−80 wt % ($0.1x - 0.4x$) sulfuric acid. The spectra (Figure 7) show that for as little as $0.10x$ sulfuric acid (Figure 7(D)), the free-OH signal from water is greatly reduced. This signal is absent at higher concentrations, indicating a lack of dangling hydrogen atoms at the surface for stratospherically relevant concentrations.

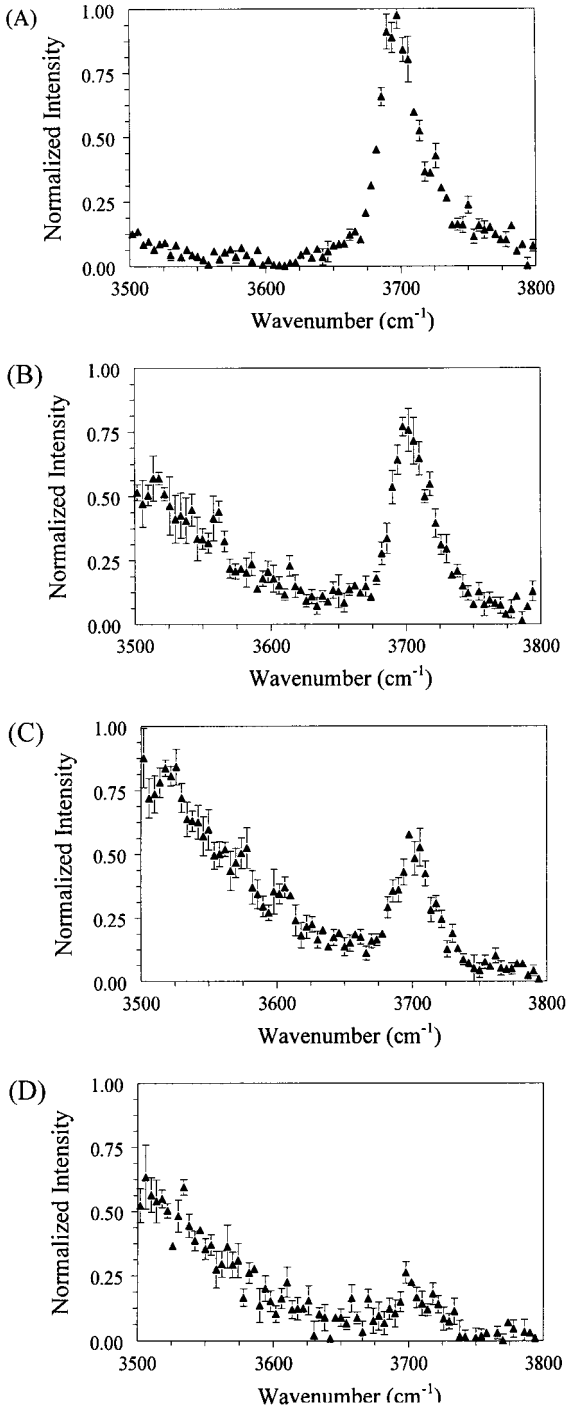

Figure 7. Free water on aqueous sulfuric acid solutions (A) $0.00x$, (B) $0.01x$, (C) $0.05x$, and (D) $0.10x$ sulfuric acid. 0 °C, *ssp* polarization.

Application of multiple techniques completes the picture of water at this surface and illustrates the true power of surface science. Somorjai and co-workers[31,32] have examined sulfuric acid solutions containing 25 to 100 wt % ($0.06x - 1.0x$) sulfuric acid using X-ray photoelectron spectroscopy (XPS) and Auger electron spectroscopy (AES). The surface S:O ratio reflects that of the bulk. Although sulfuric acid is commonly thought of as a strong electrolyte, at high concentrations the oppositely charged ions form associated ion pairs. Phillips[87] calculates that the dominant form of sulfuric acid and water in $0.2x$ sulfuric acid consists of molecular hydrates. In more detail, Heyrovská[88] has calculated the degree of association in the bulk solution. When the oppositely charged ions associate, the neutral

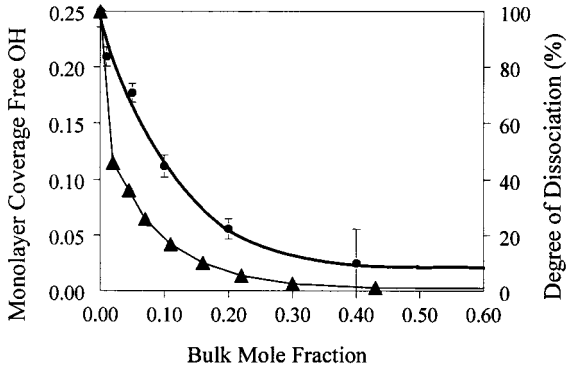

Figure 8. Free-OH stretch of water on aqueous sulfuric acid (●) decreases with the sulfuric acid degree of dissociation (▲).

complexes can penetrate to the top monolayer of the solution, displacing water and decreasing the free-OH signal. Accordingly, there is a strong correlation between the degree of ion association and decrease of the free-OH signal from water (Figure 8). Combined, the three techniques (SFG, XPS, and AES) suggest that water in the surface is bound in hydrates.

The emerging view is that water on the surface of sulfuric acid solutions is bound in sulfate hydrates at concentrations relevant to stratospheric conditions. To determine if the lower temperatures of the stratosphere result in greater partitioning of water to the surface, surface water was examined as a function of temperature for a 0.2*x* solution.[81] Neither hydrogen-bonded water (discussed in the next section) nor the free-OH water is significantly altered for temperatures as low as 216 K. The degree of ionization affects the mechanism for stratospheric heterogeneous reactions[89] and this result suggests that ionization in the surface layer does not change with temperature.

To investigate penetration to the surface by associated ion pairs, a series of alkali bisulfate and sulfate salts were investigated, keeping the molecular mole fraction constant at 0.01*x*. The sulfate ion has a higher charge density than the bisulfate ion, so is surrounded by a larger number of solvating water molecules. Sulfate salts thus less readily form neutral ion-pairs. The sulfate salts therefore retain a charge and are energetically disfavored in the top layer, and less likely to displace first-layer water molecules. Consistent with this model, the sulfate-salt spectra (Figure 9B) have a higher free-OH intensity than the corresponding bisulfate salts (Figure 9A).

A similar pattern is observed as the cation size is varied. Li^+ is the smallest cation in the series. The lithium ion salt spectra show the least suppression of the free-OH stretch, indicating little penetration to the surface even for the bisulfate salt. The small Li^+ ion is readily hydrolyzed and associates little with the counterion in solution. K^+ is intermediate in size between Li^+ and Cs^+, and the potassium salt spectra show the greatest difference between the bisulfate (Figure 9A) and the sulfate (Figure 9B). K^+ associates to a greater degree with the less highly charged HSO_4^- ion, penetrating to the top layer and displacing free water. The spectra of the largest ion, Cs^+, salts show the greatest suppression of the free-OH stretch for both ions, indicating the greatest association with the anion and penetration to the surface for both sulfate and bisulfate salts. These results are in accord with hard−soft acid−base theory which indicates greater association between large, polarizable ions than small, hard ones.[90]

5.1.3. Aqueous Ammonia. Ammonia interaction with the aqueous surface is of interest to environmental chemists in part because ammonia is the only basic, gas-phase molecule of significance in the atmosphere. Specifically, ammonia is found in aerosols only to the limit of neutralizing acidic species in the aerosol solution.[91] This limit is consistent with the conjectured surface complex between ammonia and water, first postulated by Rice[22] in 1928 based on surface tension data. On acidic solutions, NH_3 protonates to NH_4^+ and the ion partitions to the interior. At a neutral pH, molecular NH_3 occupies the

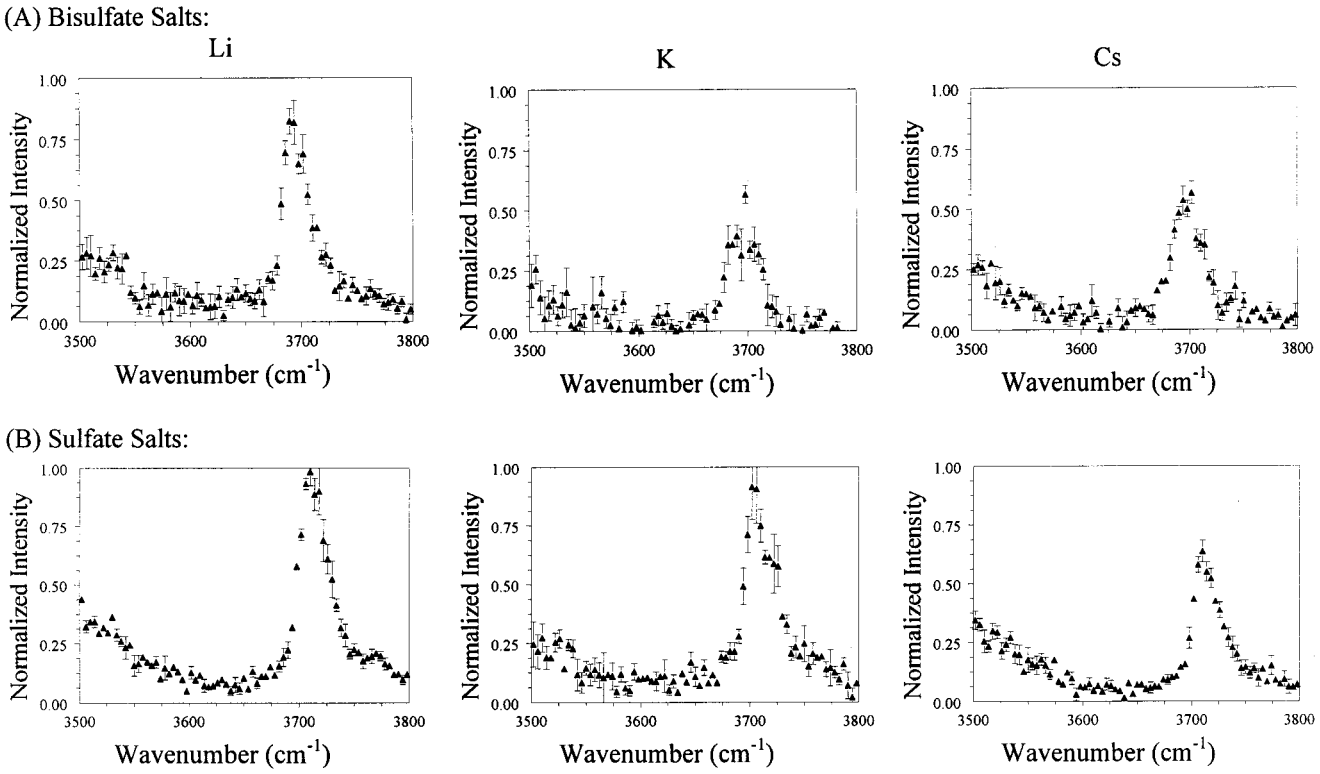

Figure 9. Free-OH spectra for aqueous alkali (A) bisulfate and (B) sulfate salt solutions, concentration 0.01*x*. All spectra are *ssp* and normalized to the incident infrared intensity and referenced to the free-OH stretch of neat water. Temperature: 0 °C.

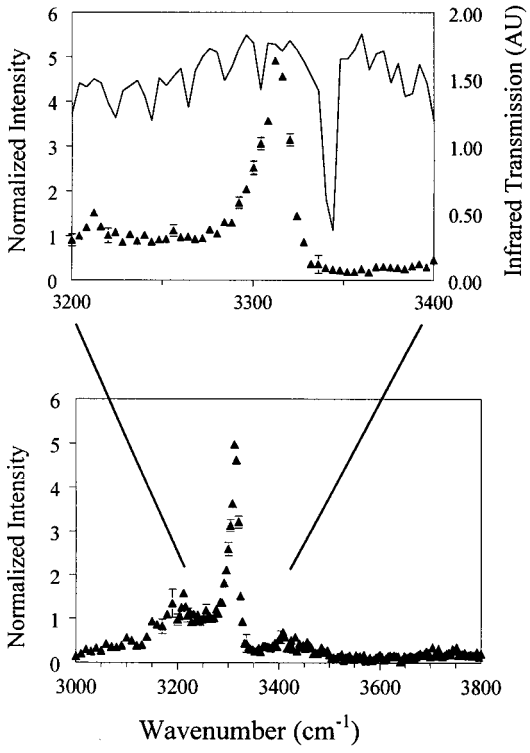

Figure 10. SFG spectrum (*ssp* polarization) of aqueous ammonia (▲) compared with the gas-phase absorption (—) obtained simultaneously through the headspace port.

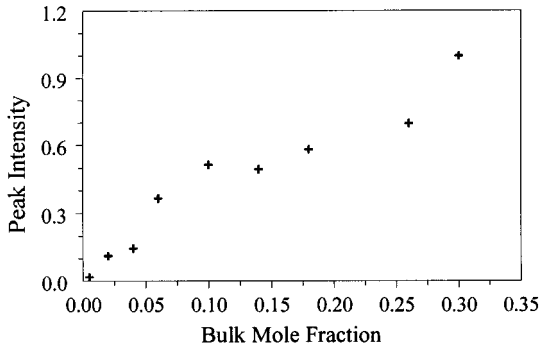

Figure 11. Surface versus bulk mole fraction ammonia for aqueous ammonia solution. The ammonia peak intensity increases with bulk mole fraction in three distinct regions. From 0 to 0.10*x* ammonia surface concentration increases sharply with bulk concentration. From 0.10−0.25*x* the surface concentration increases little despite more than doubling the bulk concentration. Above 0.25*x*, the surface concentration again increases sharply.

surface sites, inhibiting further adsorption of ammonia. This conjectured surface complex was largely neglected until recent uptake measurements[92−95] invoked a surface complex to model the uptake coefficient. The SFG spectrum of the aqueous ammonia surface (Figure 10) provides the first, direct molecular-level measurement of this complex.[82] Addition of NH_3 to water introduces an intense, narrow resonance at 3312 cm^{-1}, which is readily identified as the symmetric stretch of ammonia. This resonance is only slightly red shifted from the gas-phase resonance at 3333 cm^{-1} (inset, Figure 10) indicating little perturbation of the N−H bonding in ammonia as a result of adsorption to the surface.

Analysis of the peak intensity versus bulk mole fraction (Figure 11) indicates three distinct concentration regions: ≤0.10*x*, 0.10*x* to 0.25*x*, and >0.25*x*. Further, below 0.10*x*, the ammonia resonance increases as the free-OH resonance decreases.[96] This tradeoff suggests that at low concentration, ammonia titrates the free-OH bonds, simply docking to the dangling hydrogen through the ammonia lone pair. A similar picture emerges from a combination of ab initio calculations and surface tension measurements.[97] When half the free-OH groups are decorated with ammonia, the decline of the free-OH resonance is arrested until the ammonia bulk concentration doubles (>0.20*x*). A recent report of calculations for ammonia on ice[98] similarly finds that ammonia absorption on ice saturates when half the dangling-OH groups are decorated with ammonia. Further work is underway to determine the formation energy in each of these three regions and the interactions that separate them.

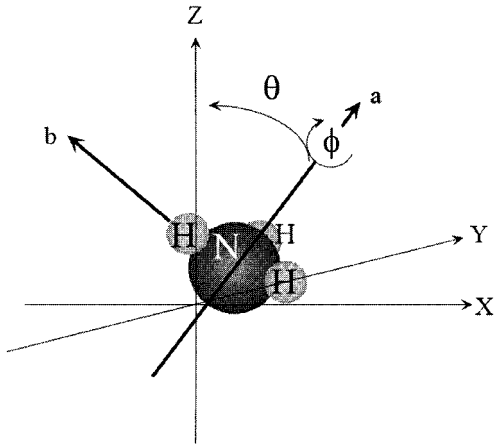

Figure 12. Orientation of ammonia on aqueous ammonia: the C_3 axis is tilted, on average, 38° from the normal.

On dielectric surfaces, SFG is most often used to obtain the vibrational spectra of surface species using *ssp* polarization. Occasionally, other polarization combinations are used to determine orientation of particular species on the surface. For ammonia, the symmetric and antisymmetric NH_3 stretches are orthogonal, and an intensity comparison can serve to identify the orientation. Although hampered somewhat by the weak Raman cross section of the antisymmetric stretch, the orientation can be ascertained by comparison of the *ssp* and *ppp* SFG spectra. Observed intensity with a single polarization combination often results in a wide range of possible orientations. However, the intersection of the range from several orientations can restrict the possible orientations. For aqueous ammonia, the combined measurements indicate that ammonia is tilted, on average, between 25° and 38° from the normal. This configuration is shown by the cartoon in Figure 12. It should be noted that ammonia is not static. In particular, a lack of splitting in the asymmetric stretch resonance indicates free rotation about the C_3 axis. Further, this orientation represents the average orientation of the surface ensemble.

Water at the aqueous ammonia interface is examined by focusing on the free-OH resonance as the ammonia concentration increases (Figure 13). The free OH consists of two components. The narrow resonance at 3700 cm^{-1} becomes narrower with as little as 0.005*x* NH_3 and disappears with 0.04*x* NH_3 (not shown). A broader peak (Figure 13C) extends for nearly 100 cm^{-1} beginning at 3680 cm^{-1} and persists to very high ammonia concentration (0.33*x*). This is the first report of this broad free-OH feature on the aqueous surface. Facile interaction with the narrower feature identifies these free-OH groups as the readily accessible, dangling hydrogen atoms. A similar docking of NH_3 to the readily accessible dangling hydrogen atoms on low-temperature ice has been reported by

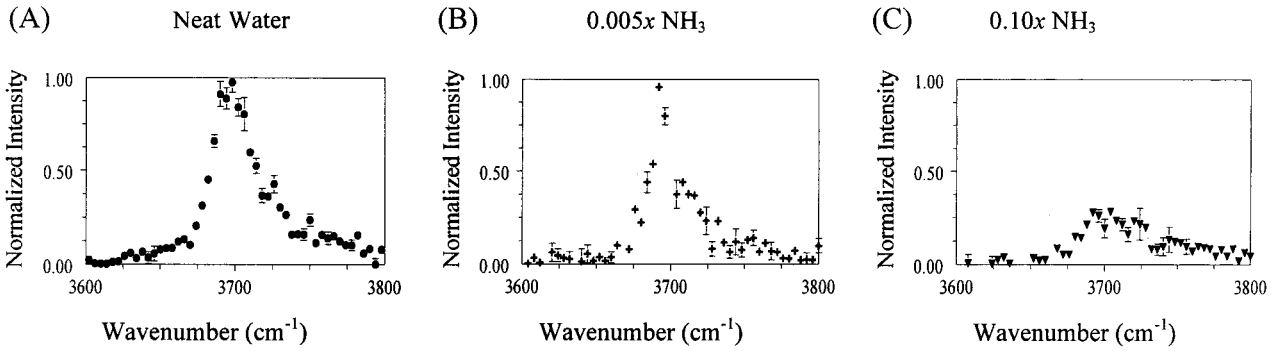

Figure 13. Free-OH resonance of water (A) narrows and decreases with as little as 0.005*x* NH_3 (B). The broader resonance, shown for 0.10*x* NH_3 (C) persists to high concentration.

Buch and Devlin.[38,99] Orientation of ammonia tilted at slightly over 30° is consistent with these hydrogen atoms dangling from water molecules with both lone pairs and the remaining hydrogen involved in hydrogen bonding in the surface. Further modeling and spectroscopic studies are required to identify the less available dangling-OH bonds. Ammonia, thus serves as a very sensitive, test-probe of the configuration of water at the surface.

5.2. Subsurface Bilayer: Acids vs Salts. The free-OH stretch necessarily responds only to perturbations that reach the very top monolayer of the surface or species that are actually present in the top monolayer. In contrast, hydrogen-bonded water is affected well beyond the top monolayer. Indeed as long as the water molecules are polar ordered, i.e., not randomly distributed, isotropic symmetry is broken and these water molecules contribute to the SFG intensity. An open issue in SFG is determination of the depth of this polar ordering. Nonetheless, examination of the hydrogen-bonded region of water probes the response of water in the top layers to species in solution. Two models have been proposed to account for variation of the intensity in the hydrogen-bonded region when salts or acids are added to water, and these have quite different ramifications for interactions between the surface and incoming, gas-phase reactants. In one model, water molecules rotate. Rotation presents the oxygen lone pair to impinging gas-phase species, a favorable configuration for hydrogen bond donors. In the alternate model, the molecules do not rotate, but the spectral intensity is enhanced by the field from the ions. These diverse models are discussed further below after presentation of the spectra.

Figure 14 shows the SFG spectrum from 3000 to 3800 cm^{-1} for representative aqueous solutions. (The spectrum of water is included in panel E for reference.) The anion (HSO_4^-) concentration was kept constant at 0.01*x* for all the samples. The sulfuric acid spectrum, panel A shows the typical striking intensity increase associated with acidic solutions, particularly for the 3150 cm^{-1} peak. Similar increases are seen for HCl,[100,101] and HNO_3[101,102] solutions. Salts[79,80,101] show a less dramatic but similar intensity increase as shown in panels B−D. This intensity increase is attributed to an electric double layer that arises in the solution due to the differential distribution of anions and cations near the surface.[103−105] In all salts studied to date, the anion is larger and more polarizable than the cation. The hydration shell of the cation is therefore more strongly associated than that of the anion, limiting the approach of the cation toward the surface. Similarly, the greater polarizability of the anions results in a lower enthalpic drive of anions away from the interface. As a result, the tail of the anion distribution extends further toward the interface than that of the cation. This differential distribution gives rise to a double layer just below the surface, and the negative pole of the double layer is directed at the surface.

This model suggests that smaller cations, H^+ and Li^+, Figure 14 panels A and B, respectively, with HSO_4^- create a stronger field, and therefore a greater enhancement of the 3150 cm^{-1} peak. For the larger cations, K^+ and Cs^+ at 0.01*x*, the picture is complicated due to ion pair formation and penetration to the surface. As shown in Figure 14 panels C and D, the free-OH peak is diminished for both $CsHSO_4$ and $KHSO_4$.

Both proposed models accounting for the increased hydrogen-bonded intensity incorporate the double-layer. In the rotation model, the double layer orients the hydrogen-bonded water so that the hydrogen atoms point more directly into the bulk, increasing the projection of the dipole onto the surface normal. Because *ssp* polarization picks up the infrared dipole along the surface normal, the intensity is enhanced. In the alternate model, the dipole field created by the double layer enhances the symmetry breaking of the surface, enhancing the macroscopic infrared dipole in the surface layer. In the bulk, the isotropic molecular distribution reduces the macroscopic infrared dipole field to zero; hence, in the dipole approximation, there is no SFG from the bulk solution. Enhancement of the infrared dipole field at the surface increases the SFG intensity generated.

The two models have different implications for the surface. In one, water molecules reorient making the hydrogen atoms less accessible at the surface. In the alternate model, water molecules do not reorient and the hydrogen atom or lone pair accessibility at the surface is unaltered. Experiments are currently underway to distinguish these models.

6. Current Picture of the Aqueous/Air Interface

SFG has proven to be an excellent probe of the aqueous-air interface, providing a detailed picture of interactions in the top monolayer. At the neat water interface, the water molecules are oriented, on average, with the hydrogen atoms pointing slightly into the bulk.[48] About 20% of surface water molecules have a dangling hydrogen atom.[53] Using ammonia as a chemical probe of these dangling hydrogen atoms reveals that two distributions contribute to the resonance at 3700 cm^{-1}. One set consists of hydrogen atoms that are readily accessible to bond with the lone pair on nitrogen and are titrated by ammonia. The second set is more robust and remains to high ammonia concentrations.

Sulfuric acid forms strong hydrogen bonds and displaces unperturbed water on the surface. At concentrations relevant to stratospheric chemistry, the surface of aqueous sulfuric acid is depleted of free water. On hygroscopic liquids, the surface monolayer is an energetically unfavorable location for water, and the surface is depleted of water for a low mole fraction of solute.

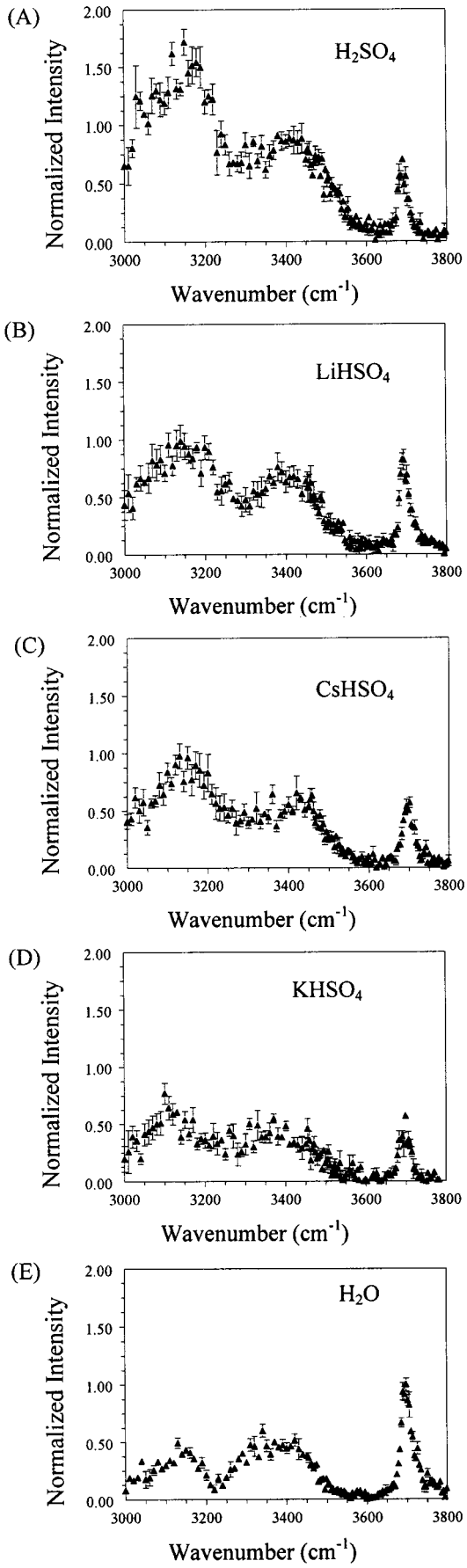

Figure 14. Hydrogen-bonded region of water is strongly dependent on the inorganic ions in solution. All spectra at 0 °C, polarization *ssp*, A−D concentration 0.01*x*. (A) H_2SO_4, (B) $LiHSO_4$, (C) $CsHSO_4$, (D) $KHSO_4$, and (E) H_2O.

Salts in solution form a double layer at the surface due to the differential distribution of the anions and the cations near the surface. The double layer enhances the SFG intensity. Two models have been proposed for this enhancement: a rotational model in which water molecules reorient in response to the field, and a field enhanced dipole moment model in which symmetry breaking due to the double layer enhances the infrared transition dipole. Distinguishing these models requires further experimental measurements and theoretical calculations.

7. Future Prospects

7.1. SFG. SFG on soft interfaces is a relatively young field and the limits of applicability have not yet been established. Major outstanding issues are associated with scale. Generation of the sum frequency depends on properties that change on two different scales: the change in the index of refraction at the interface and the wavelength of the probe radiation. The index of refraction is a macroscopic property of a medium, but the electron density giving rise to the index changes on a molecular scale at the interface. The coherence length of the probe, determined by the wavelength of the visible beam, is several orders of magnitude larger than the scale over which the index changes. Determining orientation from polarization data often depends on the index of refraction, complicating the analysis and limiting applicability. A combination of theoretical[64,65,106] and experimental efforts clarifying this technical issue is needed.

SFG does not inherently give information on the depth probed. Future experimental and theoretical efforts are needed to determine this depth. Knowing the ordering depth is important, for example, in understanding catalytic processes, for control of reactions, and for probing the scale of the hydration shell around ions and biologically relevant molecules.

7.2. Aqueous Interface. For aqueous solutions, a combination of theoretical and experimental methods are just converging to elucidate the two major open questions involving aqueous interfaces: How does solution formation change the molecular-level distribution and orientation of surface molecules? How are the dynamics at the surface affected by the molecular-level changes? The surprising result of the experimental work is that inorganic ions in solution have a profound affect on the vibrational spectrum of water on the surface. However, a comprehensive understanding of the mechanism and therefore the implications of this affect is lacking. Molecular dynamics simulations support the notion of a subsurface double layer[108,109] with ion-pair formation at high concentration.[11] The effect of this double layer field on the water molecules is, however not understood. Rotation of the surface molecules in response to the field implies a less robust hydrogen-bonded network than the field enhanced vibrational dipole model. Because the cooperative nature of the hydrogen bonding network on the aqueous surface is germane to aqueous chemistry from deep sea to interstellar space to biomolecular processes deep within the body, there is widespread motivation to develop this understanding.

There are a number of directions that the study of aqueous interfaces could take to develop this understanding. Molecular dynamics simulations coupled with experimental measurements will probably continue to contribute. As of this date, the simulations have not simulated the intensity enhancement due to ions. Ions in solution present a significant challenge due to the long range nature of the Coulombic field. Refining the simulations to include the structure of a large number of water molecules is necessary to simulate dielectric shielding due to the hydration shell. Because these refinements are also ap-

plicable to determination of the structure of macromolecular biomolecules in aqueous solution, there is a considerable payoff. Experimentally, it is possible that a combination of surface sensitive spectroscopy and dynamics will distinguish the two models of surface water and simultaneously determine energetics at the surface.[110] It will be important to judiciously choose the molecular probe for a clean answer.

As more general and reliable pulsed infrared sources are developed, experimental efforts will likely generate more detailed data to challenge understanding of the surface. For example, the results from glycerol and ammonia, discussed in this paper, provide a picture of the interface because both solute and water are detected. For the sulfate and bisulfate systems, generation of long wavelength infrared will enable detection of these materials, filling in the picture of the interface. The ultimate challenge is to determine the effect of solutes on the hydrogen-bonding network at the interface of this extremely important aqueous system.

Acknowledgment. The work reported here was supported in part from grants from the National Science Foundation (Nos. CHE-9816380 and CHE-9208232), the United States Environmental Protection Agency (No. R822453), and the Tufts University Faculty Research Fund.

References and Notes

(1) Robinson, G. W.; Zhu, S.-B.; Singh, S.; Evans, M. W. *Water in Biology, Chemistry and Physics, Experimental Overviews and Computational Methodologies*; World Scientific: Singapore, 1996.
(2) Xantheas, S. S. *Chem. Phys.* **2000**, *258*, 225−231.
(3) Peslherbe, G. H.; Ladanyi, B. M.; Hynes, J. T. *Chem. Phys.* **2000**, *258*, 201−224.
(4) Cao, Y.; Choi, J.-H.; Haas, B.-M.; Matthew, S. J.; Okumura, M. *J. Chem. Phys.* **1993**, *99*, 9307.
(5) Ayotte, P.; Weddle, G. H.; Kim, J.; Johnson, M. A. *J. Am. Chem. Soc.* **1998**, *120*, 12 361−12 362.
(6) Ayotte, P.; Bailey, C. G.; Weddle, G. H.; Johnson, M. A. *J. Phys. Chem. A* **1998**, *102*, 3067−3071.
(7) Ayotte, P.; Weddle, G.; Kim, J.; Johnson, M. A. *Chem. Phys.* **1998**, *239*, 485−491.
(8) Johnson, M. S.; Kuwata, K. T.; Wong, C.-K.; Okumura, M. *Chem. Phys. Lett.* **1996**, *260*, 551−557.
(9) Finlayson-Pitts, B. J. *Res. Chem. Intermed.* **1993**, *19*, 235−249.
(10) Finlayson-Pitts, B. J.; Hemminger, J. C. *J. Phys. Chem. A* **2000**, *104*, 11 463−11 477.
(11) Knipping, E. M.; Lakin, M. J.; Foster, K. L.; Jungwirth, P.; Tobias, D. J.; Gerber, R. B.; Dabdub, D.; Finlayson-Pitts, B. J. *Science* **2000**, *288*, 301−306.
(12) Oum, K. W.; Lakin, M. J.; DeHaan, D. O.; Bauers, T.; Finlayson-Pitts, B. J. *Science* **1998**, *279*, 74−77.
(13) Spicer, C. W.; Chapman, E. G.; Finlayson-Pitts, B. J.; Plastridge, R. A.; Hubbe, J. M.; Fast, J. D.; Berkowitz, C. M. *Nature* **1998**, *394*, 353−356.
(14) Hanson, D. R.; Ravishankara, A. R. *J. Geophys. Res.* **1991**, *96*, 17 307−17 314.
(15) Turco, R. P.; Whitten, R. C.; Toon, O. B. *J. Geophys. Space Phys.* **1982**, *20*, 233−279.
(16) Zhang, R.; Leu, M.-T.; Keyser, L. F. *J. Phys. Chem.* **1994**, *98*, 13 563−13 574.
(17) Wolff, E. W.; Mulvaney, R. *Geophys. Res. Lett.* **1991**, *99*, 3615−3629.
(18) Onsager, L.; Samaras, N. N. T. *J. Chem. Phys.* **1934**, *2*, 528−536.
(19) Randles, J. E. B. *Phys. Chem. Liq.* **1977**, *7*, 107−179.
(20) Harkins, W. D.; McLaughlin, H. M. *J. Am. Chem. Soc.* **1925**, *47*, 2083.
(21) Harkins, W. D.; Gilbert, E. C. *J. Am. Chem. Soc.* **1926**, *48*, 604.
(22) Rice, O. K. *J. Phys. Chem.* **1928**, *32*, 583−592.
(23) Bernal, J. D.; Fowler, R. H. *J. Chem. Phys.* **1933**, *1*, 515−548.
(24) Sabinina, L.; Terpugow, L. *Z. Phys. Chem. Abt. A* **1935**, *173*, 237−248.
(25) Adamson, A. W.; Gast, A. P. *Physical Chemistry of Surfaces*; 6th ed.; John Wiley and Sons: New York, 1997.
(26) Tassotto, M.; Gannon, T. J.; Watson, P. R. *J. Chem. Phys.* **1997**, *107*, 8899−8903.
(27) Benjamin, I.; Wilson, M. A.; Pohorille, A.; Nathanson, G. M. *Chem. Phys. Lett.* **1995**, *243*, 222−228.
(28) Klassen, J.; Fiehrer, K. M.; Nathanson, G. M. *J. Phys. Chem.* **1997**, *101*, 9098−9106.
(29) Morris, J. R.; Behr, P.; Antman, M. D.; Ringeisen, B. R.; Splan, J.; Nathanson, G. M. *J. Phys. Chem. A* **2000**, *104*, 6738−6751.
(30) Nathanson, G.; Davidovits, P.; Worsnop, D.; Kolb, C. *J. Phys. Chem.* **1996**, *100*, 13 007.
(31) Fairbrother, D. H.; Johnston, H.; Somorjai, G. *J. Phys. Chem.* **1996**, *100*, 13 696−13 700.
(32) Fairbrother, D. H.; Somorjai, G. A. *J. Phys. Chem. B* **2000**, *104*, 4649−4652.
(33) Behr, P.; Morris, J. R.; Antman, M. D.; Ringeisen, B. R.; Splan, J. P.; Nathanson, G. M. *Geophys. Res. Lett.* **2001**, *28*, 1961−1964.
(34) Yang, H.; Finlayson-Pitts, B. J. *J. Phys. Chem. A* **2001**, *105*, 1890−1896.
(35) Hernandez, J.; Uras, N.; Devlin, J. P. *J. Chem. Phys.* **1998**, *108*, 4525−4529.
(36) Delzeit, L.; Powell, K.; Uras, N.; Devlin, J. P. *J. Phys. Chem. B* **1997**, *101*, 2327−2332.
(37) Devlin, J. P.; Buch, V. *J. Phys. Chem. B* **1997**, *101*, 6095−6098.
(38) Buch, V.; Delzeit, L.; Blackledge, C.; Devlin, J. P. *J. Phys. Chem.* **1996**, *100*, 3732−3744.
(39) Rowland, B.; Kadagathur, N. S.; Devlin, J. P.; Buch, V.; Feldman, T.; Wojcik, M. J. *J. Chem. Phys.* **1995**, *102*, 8328−8341.
(40) Bloembergen, N.; Pershan, P. S. *Phys. Rev.* **1962**, *128*, 606−622.
(41) Shen, Y. R. *Ann. Rev. Phys. Chem.* **1989**, *40*, 327−350.
(42) Eisenthal, K. B. *Chem. Rev.* **1996**, *96*, 1343−1360.
(43) Gragson, D. E.; Richmond, G. L. *J. Phys. Chem. B* **1998**, *102*, 3847−3861.
(44) Miranda, P. B.; Shen, Y. R. *J. Phys. Chem. B* **1999**, *103*, 3292−3307.
(45) Shultz, M. J.; Schnitzer, C.; Simonelli, D.; Baldelli, S. *Int. Rev. Phys. Chem.* **2000**, *19*, 123−153.
(46) Heinz, T. F.; Tom, H. W. K.; Shen, Y. R. *Phys. Rev. A* **1983**, *28*, 1883−1885.
(47) Higgins, D. A.; Byerly, S. K.; Abrams, M. B.; Corn, R. M. *J. Phys. Chem.* **1991**, *95*, 6984−6990.
(48) Goh, M. C.; Hicks, J. M.; Kemnitz, K.; Pinto, G. R.; Bhattacharyya, K.; Eisenthal, K. B.; Heinz, T. F. *J. Phys. Chem.* **1988**, *92*, 5074−5075.
(49) Hunt, J. H.; Guyot-Sionnest, P.; Shen, Y. R. *Chem. Phys. Lett.* **1987**, *133*, 189−192.
(50) Guyot-Sionnest, P.; Superfine, R.; Hunt, J. H.; Shen, Y. R. *Chem. Phys. Lett.* **1988**, *144*, 1.
(51) Harris, A. L.; Chidsey, C. E. D.; Levinos, N. J.; Loiacono, D. N. *Chem. Phys. Lett.* **1987**, *141*, 350.
(52) Superfine, R.; Huang, J. Y.; Shen, Y. R. *Phys. Rev. Lett.* **1991**, *66*, 1066.
(53) Du, Q.; Superfine, R.; Freysz, E.; Shen, Y. R. *Phys. Rev. Lett.* **1993**, *70*, 2313−2316.
(54) Conboy, J. C.; Messmer, M. C.; Richmond, G. L. *J. Phys. Chem.* **1995**, *100*, 7617.
(55) Gragson, D. E.; Richmond, G. L. *J. Chem. Phys.* **1997**, *107*, 9687−9690.
(56) Gragson, D. E.; Richmond, G. L. *J. Phys. Chem. B* **1998**, *102*, 569−576.
(57) Messmer, M. C.; Conboy, J. C.; Richmond, G. L. *J. Am. Chem. Soc.* **1995**, *117*, 8039.
(58) Dick, B.; Gierulski, A.; Marowsky, G.; Reider, G. A. *Appl. Phys. B.* **1985**, *38*, 107−116.
(59) Dick, B. *Chem. Phys.* **1985**, *96*, 199−215.
(60) Hirose, C.; Akamatsu, N.; Domen, K. *Appl. Spec.* **1992**, *46*, 1051−1072.
(61) Hirose, C.; Akamatsu, N.; Domen, K. *J. Chem. Phys.* **1992**, *96*, 997−1004.
(62) Muenchausen, R. E.; Keller, R. A.; Nogar, N. S. *J. Opt. Soc. Am.* **1987**, *4*, 237−241.
(63) Akamatsu, N.; Domen, K.; Hirose, C. *Appl. Spec.* **1992**, *46*, 1051−102.
(64) Morita, A.; Hynes, J. T. *Chem. Phys.* **2000**, *258*, 371−390.
(65) Morita, A.; Hynes, J. T. *J. Phys. Chem.* **2001**, *B*, 1−36.
(66) Chen, H.; Irish, D. E. *J. Phys. Chem.* **1971**, *75*, 2672−2681.
(67) Irish, D. E.; Chen, H. *J. Phys. Chem.* **1970**, *74*, 3796−3802.
(68) Irish, D. E.; Brooker, M. H. *Raman and Infrared Spectral Studies of Electrolytes*; Clark, R. J. H. and Hester, R. E., Ed.; Heyden & Son: London, 1981, pp 212−311.
(69) Ratcliffe, C. I.; Irish, D. E. *J. Phys. Chem.* **1982**, *86*, 4897−4905.
(70) Ratcliffe, C. I.; Irish, D. E. *Can. J. Chem.* **1985**, *63*, 3521−3525.
(71) Scherer, J. R. *The Vibrational Spectroscopy of Water*; Clark, R. J. H., Hester, R. E., Eds.; Heyden: Philadelphia, 1978; Vol. 5, pp 149−216.
(72) Scherer, J. R.; Go, M. K.; Kint, S. *J. Phys. Chem.* **1974**, *78*, 1304−1313.
(73) Buch, V.; Devlin, J. P. *J. Chem. Phys.* **1999**, *110*, 3437−3443.

(74) Devlin, J. P.; Buch, V. *J. Phys. Chem.* **1995**, *99*, 16 534−16 548.
(75) Devlin, J. P.; Joyce, C.; Buch, V. *J. Phys. Chem. A* **2000**, *104*, 1974−1977.
(76) Tsai, C. J.; Jordan, K. D. *J. Phys. Chem.* **1993**, *97*, 5208−5210.
(77) Baldelli, S.; Schnitzer, C.; Shultz, M. J.; Campbell, D. *J. Phys. Chem. B* **1997**, *101*, 4607−4312.
(78) Baldelli, S.; Schnitzer, C.; Shultz, M. J.; Campbell, D. *J. Phys. Chem. B* **1997**, *101*, 10 435−10 441.
(79) Baldelli, S.; Schnitzer, C.; Shultz, M. J.; Campbell, D. J. *Chem. Phys. Lett.* **1998**, *287*, 143−147.
(80) Baldelli, S.; Campbell, D.; Schnitzer, C.; Shultz, M. J. *J. Phys. Chem. B* **1999**, *103*, 2789−2795.
(81) Schnitzer, C.; Baldelli, S.; Shultz, M. J. *Chem. Phys. Lett.* **2000**, *313*, 416−420.
(82) Simonelli, D.; Baldelli, S.; Shultz, M. J. *Chem. Phys. Lett.* **1998**, *298*, 400−404.
(83) Simonelli, D.; Shultz, M. J. *J. Chem. Phys.* **2000**, *112*, 6804−6816.
(84) Miner, C. S.; Dalton, N. N. *Glycerol*; Reinhold Publishing Corp.: New York, 1953.
(85) Chattoraj, D. K.; Moulik, S. P. *Ind. J. Chem.* **1977**, *15a*, 73−79.
(86) Saecker, M. E.; Nathanson, G. *J. Chem. Phys.* **1993**, *99*, 7056−7075.
(87) Phillips, L. F. *Aust. J. Chem.* **1994**, *47*, 91−100.
(88) Heyrovská, R., Degree of Dissociation of Sulfates of Monovalent Cations in Aqueous Solutions, personal communication.
(89) Zhang, R.; Wooldridge, P. J.; Abbatt, J. P. D.; Molina, M. J. *J. Phys. Chem.* **1993**, *97*, 7351−7358.
(90) Butler, J. N. *Ionic Equilibrium: Solubility and pH Calculations*; Revised ed.; Wiley Interscience: New York, 1998.
(91) Bates, T. S.; Huebert, B. J.; Gras, J. L.; Griffths, F. B.; Durkee, P. A. *J. Geophys. Res.* **1998**, *103*, 16 297−16 318.
(92) Bongartz, A.; Schweighoefer, S.; Roose, C.; Schurath, U. *J. Atmos. Chem.* **1995**, *35*, 35−58.
(93) Ponche, J. L.; George, C.; Mirabel, P. *J. Atmos. Chem.* **1993**, *16*, 1.
(94) Shi, Q.; Davidovits, P.; Jayne, J. T.; Worsnop, D. R.; Kolb, C. E. *J. Phys. Chem. A* **1999**, *103*, 8812−8823.
(95) Swartz, E.; Shi, Q.; Davidovits, P.; Jayne, J. T.; Worsnop, D. R.; Kolb, C. E. *J. Phys. Chem. A* **1999**, *103*, 8824−5533.
(96) Simonelli, D.; Bandara; Shultz, M. J., in preparation.
(97) Donaldson, D. J. *J. Phys. Chem. A* **1999**, *103*, 62−70.
(98) Hara, Y.; Hashimoto, N. T.; Nagaoka, M. *Chem. Phys. Lett.* **2001**, *348*, 107−114.
(99) Uras, N.; Buch, V.; Devlin, J. P. *J. Phys. Chem. B* **2000**, *104*, 9203−9209.
(100) Baldelli, S.; Schnitzer, C.; Shultz, M. J. *Chem. Phys. Lett.* **1999**, *302*, 157−163.
(101) Schnitzer, C.; Baldelli, S.; Shultz, M. J. *J. Phys. Chem. B* **2000**, *104*, 585−590.
(102) Schnitzer, C.; Baldelli, S.; Campbell, D. J.; Shultz, M. J. *J. Phys. Chem. A* **1999**, *103*, 6383−6386.
(103) Jungwirth, P.; Tobias, D. J. *J. Phys. Chem. B* **2001**, 10 468−10 472.
(104) Jungwirth, P. *J. Phys. Chem. A* **2000**, *104*, 145−148.
(105) Jungwirth, P.; Tobias, D. J. *J. Phys. Chem. B* **2000**, *104*, 7702−7706.
(106) Dawidowski, J.; Bermejo, F. J.; Cabrillo, C.; Bennington, S. M. *Chem. Phys.* **2000**, *258*, 247−255.
(107) Wilson, M.; Pohorille, A. *J. Chem. Phys.* **1991**, *95*, 6005−6013.
(108) Benjamin, I. *Acc. Chem. Res.* **1995**, *28*, 233.
(109) Tobias, D. J.; Jungwirth, P.; Parrinello, M. *J. Chem. Phys.* **2001**, *114*, 7036−7044.
(110) Bhattacharyya, K.; Bagchi, B. *J. Phys. Chem. A* **2000**, *104*, 10 603−10 613.